

Synthetic Studies of Neoclerodane Diterpenes from *Salvia divinorum*: Identification of a Potent and Centrally Acting μ Opioid Analgesic with Reduced Abuse Liability

Rachel Saylor Crowley, Andrew P. Riley, Alexander M. Sherwood, Chad E. Groer, Nirajmohan Shivaperumal, Miguel Biscaia, Kelly Paton, Sebastian Schneider, Davide Provasi, Bronwyn M. Kivell, Marta Filizola, and Thomas E. Prisinzano

J. Med. Chem., **Just Accepted Manuscript** • DOI: 10.1021/acs.jmedchem.6b01235 • Publication Date (Web): 28 Nov 2016

Downloaded from <http://pubs.acs.org> on December 1, 2016

Just Accepted

“Just Accepted” manuscripts have been peer-reviewed and accepted for publication. They are posted online prior to technical editing, formatting for publication and author proofing. The American Chemical Society provides “Just Accepted” as a free service to the research community to expedite the dissemination of scientific material as soon as possible after acceptance. “Just Accepted” manuscripts appear in full in PDF format accompanied by an HTML abstract. “Just Accepted” manuscripts have been fully peer reviewed, but should not be considered the official version of record. They are accessible to all readers and citable by the Digital Object Identifier (DOI®). “Just Accepted” is an optional service offered to authors. Therefore, the “Just Accepted” Web site may not include all articles that will be published in the journal. After a manuscript is technically edited and formatted, it will be removed from the “Just Accepted” Web site and published as an ASAP article. Note that technical editing may introduce minor changes to the manuscript text and/or graphics which could affect content, and all legal disclaimers and ethical guidelines that apply to the journal pertain. ACS cannot be held responsible for errors or consequences arising from the use of information contained in these “Just Accepted” manuscripts.

1
2
3
4
5
6
7
8
9
10
11
12
13
14
15
16
17
18
19
20
21
22
23
24
25
26
27
28
29
30
31
32
33
34
35
36
37
38
39
40
41
42
43
44
45
46
47
48
49
50
51
52
53
54
55
56
57
58
59
60

Synthetic Studies of Neoclerodane Diterpenes from *Salvia divinorum*: Identification of a Potent and Centrally Acting μ Opioid Analgesic with Reduced Abuse Liability

Rachel Saylor Crowley,^{1†} Andrew P. Riley,^{2†} Alexander M. Sherwood,¹ Chad E. Groer,¹ Nirajmohan Shivaperumal,³ Miguel Biscaia,³ Kelly Paton,³ Sebastian Schneider,⁴ Davide Provasi,⁴ Bronwyn M. Kivell,³ Marta Filizola,⁴ and Thomas E. Prisinzano^{1}*

¹ Department of Medicinal Chemistry, School of Pharmacy, The University of Kansas, Lawrence, KS, USA. ² Department of Chemistry, The University of Kansas, Lawrence, KS, USA. ³ School of Biological Sciences, Centre for Biodiscovery, Victoria University of Wellington, Wellington, New Zealand.

⁴ Department of Pharmacological Sciences, Icahn School of Medicine at Mount Sinai, New York, NY, USA. [†]These authors contributed equally to this work.

prisinza@ku.edu

RECEIVED DATE (to be automatically inserted after your manuscript is accepted if required according to the journal that you are submitting your paper to)

*To whom correspondence should be addressed. Thomas E. Prisinzano, Professor and Chair, 1251 Wescoe Hall Drive, 4070 Malott Hall, Lawrence, Kansas 66045-7572. Telephone: (785) 864-3267. Fax: (785) 864-5326.

1 **Abstract.** Opioids are widely used to treat millions suffering from pain, but their analgesic utility is
2 limited due to associated side effects. Herein we report the development and evaluation of a chemical
3 probe exhibiting analgesia and reduced opioid-induced side effects. This compound, kurkinorin (**5**), is a
4
5 potent and selective μ -opioid receptor (MOR) agonist ($EC_{50} = 1.2$ nM, $>8,000$ μ/κ selectivity). **5** is a
6
7 biased activator of MOR-induced G-protein signaling over β -arrestin-2 recruitment. Metadynamics
8
9 simulations of **5**'s binding to a MOR crystal structure suggest energetically preferred binding modes that
10
11 differ from crystallographic ligands. *In vivo* studies with **5** demonstrate centrally-mediated
12
13 antinociception significantly reduced rewarding effects, tolerance, and sedation. We propose that this
14
15 novel MOR agonist may represent a valuable tool in distinguishing the pathways involved in MOR-
16
17 induced analgesia from its side effects.
18
19
20
21
22
23
24
25
26
27
28
29
30
31
32
33
34
35
36
37
38
39
40
41
42
43
44
45
46
47
48
49
50
51
52
53
54
55
56
57
58
59
60

Introduction

Pain affects nearly 115 million Americans, which is more than cancer, heart disease, and diabetes combined. Unfortunately, the use of opioids, one of the most common drug classes used to treat pain, is problematic due to their high abuse liability.¹ In 2014, an estimated 54 million people over the age of 12 had used prescription drugs, such as opioids, non-medically in their lifetimes,² and according to the Centers for Disease Control and Prevention (CDC), 2014 had the highest rate of drug overdose deaths than any year prior, with an estimated 40 Americans dying each day from overdosing on prescription painkillers.³ Thus, a strong analgesic devoid of abuse liabilities is desperately needed in an attempt to combat this trend and prevent these deaths.

The prototypical opioid, morphine, has been used for decades for the management of pain, and its powerful analgesic effects have stimulated innumerable synthetic and semi-synthetic investigations aimed at optimizing its biological effects.⁴ While these studies have resulted in most of the clinically useful treatments for pain, including codeine, oxycodone, meperidine, methadone, and fentanyl, these drugs have not been able to overcome the drawbacks associated with opioid use. All of these morphine-derived compounds are μ -opioid receptor (MOR) agonists and suffer from severe adverse effects such as sedation, tolerance, dependence, constipation, and respiratory depression.^{4a} Tolerance and dependence are particularly significant effects because they can lead to opioid addiction, which is often the most concerning effect for both patients and prescribers.⁵

Most clinically used MOR ligands are structurally similar to morphine, and they all have very similar activity profiles. To date, it has been very difficult to differentiate opioid-induced analgesic activity from abuse liability. The development of novel, non-morphine-derived scaffolds of MOR ligands may allow for this differentiation. Using the natural product salvinorin A as our novel scaffold, we present herein the design and synthesis of **5** (kurkinorin), a salvinorin A analogue that demonstrates remarkable potency and selectivity for MORs. Results from *in vitro*, *in silico*, and *in vivo* evaluations indicate **5** is a useful probe of MORs and represents a crucial step towards separating analgesic activity from the adverse effects of current opioid ligands.

Results and Discussion

Of the known, naturally occurring opioid ligands, the most structurally diverse is the κ -opioid receptor (KOR) agonist salvinorin A (**1a**) found in the leaves of the mint plant *Salvia divinorum* (Fig. 1). Most notably, **1a** lacks a basic nitrogen that was once believed to be necessary for binding to opioid receptors.⁶ The structural uniqueness of **1a** has led to several semi-synthetic studies aimed at elucidating structure-activity relationships (SAR).⁷ Among the information gained from these investigations was that the orientation of the C2 substituent can have an effect on the affinity and activity at KORs.⁸ It was also demonstrated that replacement of the C2 acetate with a benzoate resulted in a loss of activity at KORs but an increase in MOR activity. This analogue, referred to as herkinorin (**2**), represents the first non-nitrogenous MOR agonist.⁹ Further evaluation of **2**'s interaction with MORs indicated that it was a functionally selective compound, as it activates MORs without promoting the recruitment of β -arrestin-2 or internalization of the receptor, both of which have been indicated to play a critical role in development of morphine-like side-effects.¹⁰ Although **2** has proven to be a useful tool for probing MORs *in vitro*¹⁰⁻¹¹ and *in vivo*,¹² it lacks sufficient potency ($EC_{50} = 39.0 \pm 4.0$ nM at MOR) and selectivity (4-fold selective for MOR over KOR) for further exploration of more complex systems of pain and drug abuse. The utility of **2** is also limited by the fact that it is peripherally restricted,^{12b} and thus cannot be used to probe centrally mediated processes.

Interestingly, the structurally similar amide **3** is significantly more potent and selective for MORs than **2**.^{11a} On the basis of molecular modeling, it was suggested that differences in receptor binding and regulation for **2** and **3** are the result of differing phenyl rings orientations.^{11a} To support this hypothesis, we have recently solved the first X-ray crystal structures for both **2** and **3** (Supplementary Fig. 1). A comparison of the two structures indicates that indeed, the phenyl ring of **3** lies more in the plane with the decalin core than the phenyl ring of **2**. Although these structures represent only two possible conformations, and not necessarily the conformations bound to the receptor, they suggested that

1 modifying the configuration of the C2 position of **2** might result in improved selectivity and potency for
2 MORs.
3

4
5 Based on the previously understood activities of **1a**, **2**, and **3** combined with this new understanding of
6 the X-ray crystal structures of **2** and **3**, it was envisioned that locking the conformation of the C2
7 substituent would impart selectivity between the MOR and KORs. The selectivity of **3** could be attributed
8 to one of two different interactions occurring due to its conformational restriction, one being the
9 coplanarity of the phenyl and decalin ring systems and the other being an upward movement of the C2
10 substituent from the α - to the β -face of the decalin core. Previous studies have demonstrated that inversion
11 of the C2 substituent of **1a** to **1c** (Scheme 1) results in a loss of activity at the KOR.^{8, 13} Thus, reduced
12 KOR activity and increased MOR activity was expected if the substituent was locked in the plane of the
13 decalin core, as seen in the crystal structure of **3**, but to determine if further movement to the β -face was
14 tolerated, or even preferred, the C2 stereochemistry had to be inverted.
15
16
17
18
19
20
21
22
23
24
25
26
27
28

29 Although the synthesis for analogues of **1a** and **2** with inverted C2 centers has been described
30 previously, **1c** and **4** (Scheme 1), respectively,¹³ the effects of this inversion on MOR and KOR activity
31 have not been fully reported. Furthermore, the introduction of an additional degree of unsaturation
32 between C2 and C3 resulting in **5** (Scheme 1), was envisioned to lock the C2 substituent in the plane of
33 the decalin core. We discuss herein the synthetic strategies employed to arrive at **5** and how these
34 modifications to the orientation of the C2 substituents affects potency and selectivity at MORs and KORs.
35
36
37
38
39
40
41
42
43
44

45 Chemical Synthesis

46
47 As mentioned above, the synthesis of compounds and **1c** and **4** have been previously reported (Scheme
48 1).¹³ Access to **5** containing the additional degree of unsaturation was envisioned to arise from the
49 oxidation of salvinorin B (**6**) to a transient diketone with subsequent tautomerization to form diosphenol
50 **7a**. Initial attempts to prepare **7a** via a Swern oxidation led to only trace amounts of product. However,
51 Cu(OAc)₂ accomplished the transformation in more acceptable yields (Scheme 1).¹⁴ Although remaining
52 **6** could be removed from the reaction mixture via silica gel chromatography, a rapid equilibration between
53
54
55
56
57
58
59
60

1 the pseudosymmetric α -diketone to the two isomeric enols **7a** and **7b** prevented further purification.
2
3 Following chromatography, immediate characterization of **7a** by NMR spectroscopy revealed a 3:1
4
5 mixture of **7a** and **7b**. However upon standing, solutions containing **7a** slowly equilibrated to
6
7 thermodynamically stable enol **7b**. Pure samples of **7b** were readily obtained.
8
9

10
11 To further explore the nature of the oxidation and tautomerization of **6**, it was determined that the action
12
13 of lead tetraacetate in MeOH/benzene on **6** produced similar mixtures of products corresponding to **7a-b**
14
15 by TLC. Following isolation of the mixture, chromatographic fractions were combined and subjected to
16
17 slow evaporation resulting in crystalline **7b**, which proved to be spectroscopically identical to the major
18
19 product obtained from the Cu(OAc)₂ reaction and was unambiguously characterized by single crystal X-
20
21 ray diffraction. Surprisingly, acylation of either the mixture of **7a-b** or pure **7b** with benzoyl chloride
22
23 provided a single regioisomer (Scheme 1), confirmed to be the desired **5** by 2D NMR studies. Briefly, the
24
25 C3 proton correlated via COSY to the C4 proton and via HMBC to C1, C2, C4, and C5. The proton of
26
27 C10 lacked any observable COSY correlations. Additionally, HSQC confirmed that carbons C3 and C10
28
29 each bear a single proton, further validating the regiochemistry of **5** (see Supplementary Fig. 2).
30
31
32
33
34

35
36 To elucidate additional SAR for this modification, two parallel series of analogues, one with and one
37
38 without saturation at the C2-C3 bond, possessing substitutions at the phenyl ring were synthesized
39
40 (Scheme 2). Due to an observed variability in the purities of commercially available acid chlorides,
41
42 commercially available carboxylic acids were coupled to **6** and **7a** through the aid of EDC and DMAP
43
44 (Scheme 1). Compounds **8a – 22a** were synthesized using a MiniBlock XT parallel synthesis system and
45
46 purified using mass-directed reverse phase HPLC. Compounds **8b – 22b** proved to be unstable to this
47
48 purification process and were synthesized in batch mode and purified using a combination of silica gel
49
50 chromatography and preparative reverse phase HPLC.
51
52
53
54
55
56
57

58 *In Vitro* Opioid Receptor Activity

59
60

1 To determine how the configuration of the C2 position in **2** affects potency and selectivity at MORs,
2 the C2-epimerized analogue **4**¹³ and the unsaturated analogue **5** were evaluated for activity at MORs and
3 KOR. Both compounds were tested for opioid activity using a functional assay that measures forskolin-
4 induced cAMP accumulation in CHO cells stably expressing either MORs KORs, or δ -opioid receptors
5 (DORs) (Table 1).¹⁵ The epimerization of **2** at the C2 position (e.g. **4**) resulted in a complete loss of
6 activity at both MOR and KORs. Of note, previously published activity profiles of **2** at KOR indicate that
7 it is a full agonist, while in this assay it appears to only be a partial agonist. Differences in the functional
8 readouts can account for these changes, and are not surprising as many compounds activate different
9 pathways to different extents. The introduction of an additional degree of unsaturation to the core of **2**,
10 however, resulted in a potent MOR agonist, **5**, with an EC₅₀ value of 1.2 ± 0.6 nM, possessing an improved
11 activity profile compared to that of **3**. Additionally, **5** was extremely selective for MORs, possessing no
12 activity at KORs at 10 μ M. This impressive >8,000-fold selectivity for MORs is drastically greater than
13 that of both **2** (4.25-fold selective over KOR) and morphine (66-fold selective over KOR). Furthermore,
14 **5** is of similar potency to DAMGO, a peptidic MOR ligand commonly employed for its high potency and
15 selectivity for MORs. **5** does have an EC₅₀ values of 74 ± 10 nM, which was unanticipated as few
16 salvinorin-like compounds have DOR activity. Even so, **5**'s MOR selectivity is still greater than 60-fold.
17 However, this result opens the possibility of identifying DOR selective neoclerodanes in the future.

18
19
20
21
22
23
24
25
26
27
28
29
30
31
32
33
34
35
36
37
38
39
40
41 To confirm that this MOR activity and selectivity cannot be attributed to the product of ester hydrolysis
42 of **5**, both **7a** and **7b** were tested for MOR and KOR activity. While **7a** cannot be fully resolved, and thus
43 fully characterized, neither compound tested showed any activity at MORs (>10,000 nM). Interestingly,
44 the 3:1 mixture of **7a**:**7b** (as characterized by ¹H NMR) was active at KORs, however pure **7b** was
45 completely inactive (Table 1).
46
47
48
49
50
51
52
53

54 Although the MOR and KORs share a high degree of similarity, the selectivity of **5** for MORs over
55 KORs supported our hypothesis that altering the conformational restriction of the C2 substituent is able
56 to grant preferential binding for one receptor over the other and thus provides a tool for designing selective
57
58
59
60

1 ligands. To further confirm the hypothesis that the KOR does not tolerate this conformational constraint,
2 the unsaturated and C2-epimerized analogues (**1b** and **1c**, respectively) of **1a** were synthesized and
3 evaluated at KOR. Compound **1b** was synthesized from **6** as described above and **1c** as described
4 previously.⁸ Neither of these changes improved potency at the KOR or resulted in MOR activity. In fact,
5 both the desaturation and the epimerization of **1a** decreased potency at the KOR by 20-fold and >3,000-
6 fold, respectively (Table 1). These data indicate that stereochemical modifications at C2 are not tolerated
7 at the KOR, and may be a reason for the high selectivity of **5** at MORs.
8
9

10 The improved potency and selectivity of **5** clearly warranted additional studies to establish SAR for
11 compounds containing this modified core, thus analogues of **2** and **5** were evaluated for their activity at
12 MORs (Supplementary Table 1). All of the analogues evaluated retained full efficacy at the MORs. In
13 all cases, the unsaturated variants were more potent than their saturated analogues, by a factor of 1.3 to
14 97-fold. A scatter plot comparison of the pEC₅₀ of the two libraries shows a clear correlation of activity
15 between the two series, indicating that parallel changes in structure correspond to parallel changes in
16 activity (Fig. 2). This correlation suggests that both the saturated and unsaturated series of analogues bind
17 at a similar location in the MORs. Generally, substitutions at the 4-position were well tolerated, with 3-
18 substituted analogues being slightly less active, and 2-substituted analogues being considerably less active
19 than the 4-substituted analogues. Of these substituted phenyl analogues, the chloro- and nitro-substituted
20 analogues were the least potent, indicating that electron-poor aromatic rings may be detrimental to
21 activity. Furthermore, none of the substituted phenyl analogues were more potent than **5**, suggesting that
22 the additional steric bulk of the substitutions is poorly tolerated and thus reduces the potency of the
23 compounds.
24
25
26
27
28
29
30
31
32
33
34
35
36
37
38
39
40
41
42
43
44
45
46
47
48
49

50 Compounds that displayed potencies below 100 nM at MORs (**8b**, **9b**, **10b**, **13b**, **16b**, **21b**, and **22b**)
51 were additionally tested at KORs and DORs to further assess their selectivity (Table 2). Compounds **8b**
52 and **10b** were the only analogues active at KOR with EC₅₀ values of 160 ± 50 and 260 ± 120 nM,
53 respectively. All of these compounds possessed weaker activity at DORs relative to MORs. Furthermore,
54
55
56
57
58
59
60

1 all analogues were less selective for MOR than **5** itself, with selectivity values ranging from 10 to 56-fold
2 and potencies ranging from 120 to 770 nM.
3

4
5 Compounds **8b**, **9b**, **10b**, **13b**, **16b**, **21b**, and **22b** were further evaluated for their ability to recruit β -
6 arrestin-2 through MOR activation. The DiscoverX (Fremont, CA) β -arrestin PathHunter™ technology
7 was used for this analysis, which utilizes enzyme fragment complementation (EFC). Both the receptor
8 and β -arrestin-2 are tagged with a fragment of β -galactosidase that is only activated upon
9 complementation. The recruitment of β -arrestin-2 to the receptor results in the activated enzyme, and the
10 addition of substrate that is converted into a luminescent product allows for a dose-dependent increase in
11 luminescence. This luminescence is then used to determine the extent of β -arrestin-2 recruitment.
12
13
14
15
16
17
18
19
20
21

22
23 DAMGO has previously been shown to highly recruit β -arrestin-2 through MOR activation,¹⁶ and was
24 thus used as the positive control to which all data were normalized. Morphine does not recruit to the same
25 extent as DAMGO, and in the EFC assay utilized herein, this trend holds true (Table 3). As mentioned
26 above, **2** has been shown to activate the MOR without recruiting β -arrestin-2,¹⁰⁻¹¹ however previous assays
27 have employed fluorescent whole-cell imaging, and in this EFC assay, **2** does weakly recruit β -arrestin-2
28 with an $EC_{50} > 3 \mu\text{M}$ and an efficacy of 72%. The previously published trend that **3** recruit β -arrestin-2
29 to a higher extent than **2** holds true in this assay, and as would be expected from its conformational
30 similarity to **3**, **5** recruits β -arrestin-2 as well. All of the **5**-like analogues tested had efficacies in the 70-
31 90% ranges, with the exception of **16b** which was more efficacious than DAMGO at 110% efficacy, but
32 **5** itself induced recruitment at the same efficacy as DAMGO.
33
34
35
36
37
38
39
40
41
42
43
44
45
46
47

48 The differing trends between **5** and its analogues in the two pathways evaluated suggest a signaling
49 bias. Much work has been done to develop models for quantifying this bias that accounts for the
50 differences between the assays and pathways,¹⁷ and a simplified equation is used herein that normalizes
51 data to the activity of DAMGO in both assays, similar to previous work^{17c, 17e} (see Experimental section
52 for full equation). Bias factor values less than 1 indicate bias towards the G-protein activation pathway
53 and those greater than 1 indicate bias towards β -arrestin-2 recruitment. As the standard to which all data
54
55
56
57
58
59
60

1 is normalized, DAMGO has a bias factor value of 1, indicating no signaling bias. The more sensitive β -
2 arrestin-2 assay used here establishes that **2** does recruit β -arrestin-2, and in fact is only slightly biased
3 towards the G-protein coupled pathway, with a bias factor of 0.95. Compounds **3** and **5** have similar
4 profiles, as originally predicted in the project rationale, having bias factor values of 0.32 and 0.57,
5 respectively, indicating a bias towards G-protein coupled pathway. The analogues of **5** are all biased
6 towards the β -arrestin-2 recruitment pathway, with bias factor values ranging from 3.1 to 9.4 Variations
7 u72in signaling bias within this small set of structurally similar compounds is intriguing, however a
8 rationale for these differences is not readily apparent and will require additional studies to more fully
9 elucidate the structure-functional selectivity relationships for this class of molecules.
10
11
12
13
14
15
16
17
18
19
20
21

22 In an effort to determine if the changes in activity may be a result of changes in the physicochemical
23 properties between the compound series, the polar surface area (PSA) and cLogP values¹⁸ as well as ligand
24 efficiency (LE) and lipophilic ligand efficiency (LELP) values were calculated (Supplementary Tables 2
25 and 3). While there are slight variations between these values for the two series, no major trends or
26 correlations are seen. The modest set of analogues outlined in this work was designed to efficiently assess
27 the SAR around the phenyl ring, and with the SAR developed from this campaign, further analogues with
28 more diverse physicochemical properties can be designed and synthesized that optimize both activity and
29 properties.
30
31
32
33
34
35
36
37
38
39
40
41
42
43
44

45 **Predicted Modes of Binding**

46 Both **2** and **5** are MOR agonists and, although structurally similar, their potency and selectivity for the
47 MOR differ significantly. These activity differences incited exploration of their binding modes at the
48 MOR. As no X-ray crystal structure of a non-nitrogenous agonist bound to the MOR has been solved yet,
49 we resorted to well-tempered multiple-walker metadynamics simulations¹⁹ to predict the energetically
50 preferred modes of binding of **2** and **5** at a flexible MOR. We previously demonstrated the ability of this
51
52
53
54
55
56
57
58
59
60

1 technique to predict accurate binding poses of opioid ligands²⁰ and described its advantages and protocol
2 in the literature.²¹
3
4

5 The analysis led to the identification of two different low-energy bound conformations for compound
6 **2** with comparable free energies. A full description of the clusters and their relative stability is reported
7 in Supplementary Table 4. Although poses 1 and 2 of **2** partially overlap with the co-crystallized ligand
8 BU72 (**23**)²² in the recently published active structure of MOR²³ (black sticks in Fig. 3), their orientation
9 in the binding pocket differs (see right panel of Fig. 3a and Supplementary Table 4 for the corresponding
10 ligand-receptor interactions). Specifically, while in pose 1 (blue in Fig. 3a), the ligand's furan ring is
11 oriented towards helices TM5 and TM6, forming hydrophobic interactions with F237^{5.44} (superscripts
12 refer to the Ballesteros-Weinstein numbering scheme²⁴) and edge-to-face interactions with H297^{6.52}, in
13 pose 2 (salmon in Fig. 3a), the ligand's furan ring points towards the receptor extracellular side, interacting
14 with I144^{3.29} and L219 in the ECL2.
15
16
17
18
19
20
21
22
23
24
25
26
27
28

29 The phenyl ring of **2** interacts with W293^{6.48} and Y326^{7.43} in pose 1, but with the latter only in pose 2,
30 in addition to Y75^{1.39} and Y128^{2.64}. In both poses, **2** interacts via water molecules with aspartic acid
31 D147^{3.32}, which usually forms a salt bridge with nitrogenous ligands. Additional interactions that are
32 occurring with high probability between the ligand and the receptor are listed in Supplementary Table 4.
33 Among them, water-mediated interactions with Y148^{3.33} and N150^{3.35} and edge-to-face interaction with
34 Y128^{2.64} are specific to pose 2, while interactions unique to pose 1 are the aforementioned interactions in
35 TM5 and 6, as well as V300^{6.55}.
36
37
38
39
40
41
42
43
44
45

46 Even larger structural variability was observed in the low-energy poses of ligand **5**, for which three
47 different poses had similar free-energies. The first two poses of **5** do not overlap with the co-crystallized
48 ligands in the active and inactive crystal structures of MOR (e.g., black lines in Fig. 3b, right panel,
49 correspond to **23**), as the ligand is located more towards the receptor extracellular side (see Supplementary
50 Table 4 for the ligand-receptor interactions formed by **5** in the three lowest-energy poses). In pose 1 (light
51 blue in Fig. 3b), **5** interacts with residues in TM1/2/6 and 7, and has the phenyl ring forming interactions
52
53
54
55
56
57
58
59
60

1 with Y75^{1.39}, Y128^{2.64}, and Y121^{7.43}. In contrast, the ligand's furan ring points towards TM6, forming
2 interactions with W318^{7.35}. Pose 2 (red sticks in Fig. 3b) represents a different orientation of **5**, with the
3 ligand's furan ring interacting with D147^{3.32}, Q124^{2.60}, and V143^{3.28} and the ligand's phenyl ring directed
4 towards Y128^{2.64}. Pose 3 of **5** is in a similar location to pose 2 of **2**, but it exhibits a different orientation
5 of the furan ring towards TM5, stabilized by a water-mediated interaction with K233^{5.40}. In this pose, the
6 ligand's phenyl ring is located closer to TM2 but it also forms interactions with Y75^{1.39} and L121^{2.57}.
7
8
9

10 Interactions that were found to be specific to compound **2** are with residues V236^{5.43}, F237^{5.44}, and
11 H297^{6.52} (pose 1), N150^{3.35} (pose 2), and Y326^{7.43} (pose 1 and 2). On the other hand, compound **5** formed
12 unique interactions with residues K303^{6.58} (pose 1); N127^{2.63}, Q124^{2.60}, V143^{3.28}, and T315^{7.32} (pose 2);
13 K233^{5.40} and Y299^{6.54} (pose 3). The ligand's phenyl ring is found to form hydrophobic interactions with
14 L121^{2.57} (a methionine in the κ -opioid receptor) during simulation of both compounds **2** (pose 2) and **5**
15 (pose 1 and 3), albeit with different probabilities (~50% for pose 2 of **2** and ~65% or ~80% for pose 1 or
16 pose 3 of **5**). As expected, the phenyl ring of **5** was observed to adopt a planar conformation with respect
17 to the decalin core, whereas it displayed a higher flexibility in the bound pose of **2**. Mutation of these
18 residues will need to be performed next to help discriminate between the energetically indistinguishable
19 poses of each ligand, discriminate between the mode of binding and/or function of **2** and **5**, and identify
20 the molecular determinants responsible for **2/5** subtype specificity.
21
22
23
24
25
26
27
28
29
30
31
32
33
34
35
36
37
38
39
40
41

42 We also used tools from the 2016-3 Schrödinger Suite (see Supporting Information for details) to
43 rationalize the observed activity variations among compound **2** derivatives (molecules **8a-22a**) and
44 compound **5** derivatives (molecules **8b-22b**). Specifically, we built a SAR model based on estimated
45 ligand-receptor interaction probabilities and the experimentally-derived EC₅₀ values reported in Table 2.
46
47
48
49
50
51

52 For each derivative, an interaction probability was obtained from weighted averages of ligand-receptor
53 interaction fingerprints of the derivative in each of their parent compound's (**2** or **5**) poses identified by
54 metadynamics (see discussion above). Specifically, the interaction fingerprints were weighted according
55 to estimated ligand binding affinities from approximated free-energy values (see details in the Supporting
56
57
58
59
60

Information). Linear regression models with no more than five regressors were ranked based on Akaike information criteria (AIC), with the smallest AIC indicating the best fitting model for the measured activities. This model (AIC=116.9) identifies ligand interaction probabilities with residues I71^{1.35}, S125^{2.62}, K233^{5.40}, V300^{6.55}, and K303^{6.58} as best at discriminating between low- and high-potency compounds (see Supplementary Fig. 7). Among these, ligand interactions with S125^{2.62} and K233^{5.40} exhibit the largest coefficients and are therefore believed to contribute more significantly to ligand potency. This model also captures the increased potency of **5**, as well as that of some of its derivatives (specifically, **9b**, **10b**, **22b**; see cluster at the bottom left of Supplementary Fig. 7). According to approximated estimates of ligand binding affinity, the most stable poses of these compounds are involved in simultaneous interaction with residues S125^{2.62} and K233^{5.40}. Notably, the less potent **2** and all its derivatives never engage in simultaneous interaction with both residues in either of the two most stable poses (see Supplementary Fig. 8, top panels), as also seen with the less potent **5** derivatives (e.g., **15b**, **17b**, and **20b**; see top right of Supplementary Fig. 7). Interestingly, all molecules based on **2** (**8a-22a**) present similar interactions with these residues in both metadynamics-derived poses: all compounds interact with K233^{5.40} but not with S125^{2.62} in pose 1, and with S125^{2.62} but not with K233^{5.40} in pose 2 (see panels on the top row of Supplementary Fig. 8). This suggests that different potencies within the herkinorin series might be affected by modulation of the ligand-receptor interaction probability, and therefore differences in binding affinity, more than by differences in allosteric coupling.

***In Vivo* Activity**

The increased potency and selectivity of **5** for the MOR relative not only to **2** but also morphine prompted further investigation into how this novel compound behaves *in vivo*. Given the historic use of MOR agonists as useful analgesics, the antinociceptive properties of **5** were investigated and compared to those of morphine and **2**.

1
2
3
4
5
6
7
8
9
10
11
12
13
14
15
16
17
18
19
20
21
22
23
24
25
26
27
28
29
30
31
32
33
34
35
36
37
38
39
40
41
42
Previously, **2** had demonstrated efficacy in both the nociceptive and inflammatory phases of the rodent formalin test.^{12b} However, these effects appeared to be limited to the site of injections, suggesting **2** is restricted to the periphery. To provide additional support of this hypothesis and determine if **5** was similarly peripherally restricted, the antinociceptive effects of both **2** and **5** were assessed in the hot water (50°C) tail-flick test in male B6-SJL mice (22-29 g), a method of testing nociceptive processes in the spinal cord.²⁵ Using this model, the centrally mediated antinociceptive effects of **2** and **5** were assessed at 1, 5, and 10 mg/kg doses alongside morphine (10 mg/kg, i.p.) with a 10 s time cutoff to prevent tissue injury. Consistent with the previous studies, **2** had no significant antinociceptive effects in the tail-flick assay (Fig. 4a). However, at 5 and 10 mg/kg doses, **5** produced a significant antinociceptive effect. Two-way repeated measures ANOVA revealed a significant effects of time $F(5,33)=64, p<0.0001$, and drug $F(5,33)=99, p<0.0001$. At the larger dose, **5** produced similar effects to that of morphine at the same dose with maximal effects observed at 30 min (Fig. 4b). Pre-treatment with the opioid antagonist naloxone (10 mg/kg s.c. 45 min) blocked the antinociceptive effects of **5** (Fig. 4b), demonstrating that these effects were opioid receptor mediated. Thus, it appears that in addition to increasing the potency and selectivity of the compound, the conversion of **2** into **5** results in a compound with the antinociceptive efficacy of morphine and the first non-nitrogenous opioid with centrally mediated antinociceptive activity. The differing abilities of **2** and **5** to penetrate the CNS is particularly surprising given the similarities not only in their structures but also their cLogP and PSA.

43
44
45
46
47
48
49
50
51
52
53
54
Although interesting and potentially promising that such a small structural change might affect *in vivo* activity so greatly, the penetration of **5** into the central nervous system may pose some additional risks. For instance, the sedation and abuse potential observed with clinically used opioids, such as morphine, are centrally mediated.²⁶ Therefore, we sought to determine if **5** would also produce similar negative side effects.

55
56
57
58
59
60
Tolerance to the analgesic effects of opioids is a major problem for pain management where increasing doses of opioids are required to maintain analgesic effects.²⁶ These escalating doses are also associated

1 with increased side effects. With this in mind, we utilized the dose-response tail-flick assay in mice using
2 a within subject design to quantify the antinociceptive effects of **5** and morphine, 30 min following each
3 cumulative dose.²⁷ Nonlinear regression analysis was used to calculate ED₅₀ values. These data show that
4
5 the two compounds are equipotent, with no significant potency differences seen between morphine (ED₅₀
6 5.3 mg/kg) and **5** (ED₅₀ 5.0 mg/kg) on day 1 (Fig. 5a, filled symbols). Differences in dose-response curves
7
8 between day 1 and day 9 were used to evaluate chronic tolerance following daily administration of either
9 morphine or **5**, (10 mg/kg/s.c.) on days 2-8. One-way ANOVA of EC₅₀ values followed by Bonferroni's
10 multiple comparison test shows that both morphine and **5** show tolerance on day 9 compared to day 1,
11 however, morphine shows significantly more tolerance on day 9 (EC₅₀ 11.6 mg/kg) compared to **5** (7.9
12 mg/kg) (Fig. 5a).
13
14
15
16
17
18
19
20
21
22
23

24 Another known side effect of morphine is its ability to produce sedation. To evaluate the sedative
25 properties of **5**, the accelerating rotarod behavioral assay in mice was used. In this assay, compounds that
26 induce motor dysfunction or sedation, such as morphine, will reduce the amount of time a test animal
27 remains on an elevated rotating rod set to accelerate from 4 to 40 rpm over 300 s (Fig. 5b). At a dose that
28 elicited maximal antinociceptive effects in the tail-flick assay (10 mg/kg), **5** demonstrated slight sedation
29 only at the 15 min time point with significantly less effect than morphine upon motor coordination overall
30 (Two-way repeated measures ANOVA shows a significant time $F(8,120)=17.18, p<0.0001$ and drug
31 interaction $F(2,15)=9.36, p<0.01$). Thus it appears that while **5** clearly acts upon the central nervous
32 system, as evidenced by its efficacy in the tail-flick test, its impairment of motor coordination is
33 considerably reduced in comparison to that of morphine. Compound **2**, which is restricted to the peripheral
34 nervous system, produced no observable effect on motor co-ordination (data not shown).
35
36
37
38
39
40
41
42
43
44
45
46
47
48
49
50

51 Finally, the rewarding effects of **5** were tested using the conditioned place preference (CPP) assay in
52 male Sprague Dawley rats (240-350 g). Following a 15 min free roaming pre-test on day 1, rats were
53 paired with either drug (morphine, **2** or **5**) or vehicle in daily 60 min conditioning sessions for 6 days
54 using a counterbalanced design. During the post-conditioning test rats were allowed to freely roam the
55
56
57
58
59
60

1 chambers for 15 min. The change in time spent in the drug-paired chamber pre- and post-conditioning is
2 shown as the CPP score (expressed as %). Using this paradigm, **5** resulted in a CPP score similar to the
3 vehicle control at both 5 mg/kg and 10 mg/kg and significantly less than the same doses of morphine (Fig.
4
5
6
7
8
9
10
11
12
13
14
15
16
17
18
19
20
21
22
23
24
25
26
27
28
29
30
31
32
33
34
35
36
37
38
39
40
41
42
43
44
45
46
47
48
49
50
51
52
53
54
55
56
57
58
59
60
6). These data indicate that **5** produces less rewarding effects than morphine, at both 5 and 10 mg/kg doses suggesting it may possess a lower liability for abuse. Taken together, the effects of **5** in animal models of antinociception, motor coordination, tolerance, and reward are very promising.

16 17 18 19 20 21 22 23 24 25 26 27 28 29 30 31 32 33 34 35 36 37 38 39 40 41 42 43 44 45 46 47 48 49 50 51 52 53 54 55 56 57 58 59 60

Through SAR studies on the naturally-occurring KOR agonist salvinorin A, we have identified **5** as a potent, selective, and centrally active probe for opioid receptors. **5**'s activation of MORs potently induces G-protein mediated effects and, to a lesser extent, recruits β -arrestin-2. Enhanced molecular dynamics simulations suggest a different mode of binding of this compound than typical opioid ligands. Interestingly, **5** has reduced tolerance, sedation, and rewarding properties compared to morphine, the standard opioid analgesic.

The molecular nature of **5**'s reduced side effect profile *in vivo* is unclear, as it does recruit β -arrestin-2 to a greater extent than morphine, but given its distinctive properties and desirable *in vivo* effects, **5** is an attractive probe for potentially differentiating analgesia from abuse liability. Furthermore, our findings provide additional evidence that moving away from morphine-based opioid ligands may serve as a viable strategy for dissociating central antinociception from common opioid induced side effects.

48 49 50 51 52 53 54 55 56 57 58 59 60

General experimental procedures. Salvinorin A was isolated from the leaves of *Salvia divinorum* and converted to **1b**, **4** and **6** as previously described.¹³ All other chemical reagents were purchased from commercial suppliers and used without further purification. All solvents were obtained from a solvent purification system in which solvent was passed through two columns of activated alumina under argon.

Reactions performed in standard glassware were performed under an atmosphere of argon using glassware dried overnight in an oven at 120 °C and cooled under a stream of argon. Reactions were monitored by thin-layer chromatography (TLC) on 0.25 mm Analtech GHLF silica gel plates and visualized using a UV Lamp (254 nm) and vanillin solution. Flash column chromatography was performed on silica gel (4–63 mm) from Sorbent Technologies. ¹H and ¹³C NMR were recorded a 500 MHz Bruker AVIII spectrometer equipped with a cryogenically-cooled carbon observe probe or a 400 MHz Bruker AVIIHD spectrometer using tetramethyl silane as an internal standard. Chemical shifts (δ) are reported in ppm and coupling constants (*J*) are reported in Hz. High-resolution mass spectrum (HRMS) was performed on a LCT Premier (Micromass Ltd., Manchester UK) time of flight mass spectrometer with an electrospray ion source in either positive or negative mode. Melting points were measured with a Thomas Capillary Melting Point Apparatus and are uncorrected. HPLC was carried out on an Agilent 1100 series HPLC system with diode array detection at 209 nm on an Agilent Eclipse XDB-C18 column (250 x 10 mm, 5 mm). Compounds were identified as ≥95% pure by HPLC before all *in vitro* and *in vivo* analyses.

*Methyl (2S,4aR,6aR,7R,10aR,10bR)-9-acetoxy-2-(furan-3-yl)-6a,10b-dimethyl-4,10-dioxo-1,4,4a,5,6,6a,7,10,10a,10b-decahydro-2H-benzo[*f*]isochromene-7-carboxylate (1b)*. A solution of **7** (37 mg, 0.095 mmol) in CH₂Cl₂ (5 mL) was treated with acetic anhydride (18 μL, 0.189 mmol), DIPEA (33 μL, 0.189 mmol), and DMAP (1.2 mg, 0.0095 mmol). After stirring overnight the reaction mixture was rinsed with HCl (1 M, 5 mL), saturated NaHCO₃ (5 mL), and brine (5 mL). The organic layer was dried over Na₂SO₄ and concentrated in vacuo. The resulting residue was purified by FCC 30%EtOAc/Pent. to yield **1b** (23 mg, 56%). ¹H NMR (500 MHz, CDCl₃) δ 7.47 – 7.34 (m, 2H), 6.52 (d, *J* = 2.2 Hz, 1H), 6.39 (dd, *J* = 1.9, 0.9 Hz, 1H), 5.62 – 5.50 (m, 1H), 3.78 (s, 3H), 3.52 (d, *J* = 2.3 Hz, 1H), 3.04 (dd, *J* = 13.7, 5.3 Hz, 1H), 2.40 (s, 1H), 2.24 (s, 3H), 2.17 (d, *J* = 5.6 Hz, 1H), 2.11 – 2.05 (m, 1H), 1.67 (ddd, *J* = 11.8, 9.7, 3.1 Hz, 3H), 1.36 (s, 3H), 1.30 – 1.24 (m, 1H), 1.17 (s, 3H). ¹³C NMR (126 MHz, CDCl₃) δ 191.00, 171.36, 170.32, 168.76, 145.21, 143.67, 139.37, 129.80, 125.41, 108.45, 72.01, 63.33, 56.35, 52.43, 51.31, 44.12, 43.72, 38.39, 35.80, 20.23, 17.91, 16.72, 14.82. HRMS calculated for C₂₃H₂₆O₈: [M+Na]⁺: 453.1539 (found); 453.1525 (calc). Melting point: = 171–175 °C (dec).

1
2
3
4
5
6
7
8
9
10
11
12
13
14
15
16
17
18
19
20
21
22
23
24
25
26
27
28
29
30
31
32
33
34
35
36
37
38
39
40
41
42
43
44
45
46
47
48
49
50
51
52
53
54
55
56
57
58
59
60

(2*S*,4*aR*,6*aR*,7*R*,10*aR*,10*bR*)-Methyl 9-((benzoyl)oxy)-2-(furan-3-yl)-6*a*,10*b*-dimethyl-4,10-dioxo-2,4,4*a*,5,6,6*a*,7,10,10*a*,10*b*-decahydro-1*H*-benzo[*ff*]isochromene-7-carboxylate (**5**). A solution of **7** (40 mg, 0.103 mmol) in CH₂Cl₂ (8 mL) was treated with benzoyl chloride (24 μL, 0.206 mmol), DIPEA (36 μL, 0.206 mmol), and DMAP (1.3 mg, 0.206 mmol). After stirring overnight the reaction mixture was rinsed with HCl (1 M, 8 mL), saturated NaHCO₃ (8 mL), and brine (8 mL). The organic layer was dried over Na₂SO₄ and concentrated in vacuo. The resulting residue was purified by FCC 30%EtOAc/Pent. to yield **5** as a white solid (26.4 mg, 52%). ¹H NMR (400 MHz, CDCl₃) δ 8.11 (d, *J* = 7.14 Hz, 2H), 7.62 (t, *J* = 7.45 Hz, 1H), 7.48 (t, *J* = 7.74 Hz, 2H), 7.41 (s, 1H), 7.39 (t, *J* = 1.66 Hz, 1H), 6.66 (d, *J* = 2.15 Hz, 1H), 6.39 (d, *J* = 0.95 Hz, 1H), 5.54 (dd, *J* = 5.28, 11.47 Hz, 1H), 3.80 (s, 3H), 3.60 (d, *J* = 2.13 Hz, 1H), 3.07 (dd, *J* = 5.34, 13.66 Hz, 1H), 2.47 (s, 1H), 2.20 (dd, *J* = 5.66, 8.50 Hz, 2H), 2.12 (m, 1H), 1.69 (m, 3H), 1.38 (s, 3H), 1.25 (s, 3H). ¹³C NMR (126 MHz, CDCl₃) δ 190.91, 171.39, 170.41, 164.61, 145.47, 143.67, 139.37, 133.94, 130.28, 129.98, 128.63, 128.28, 125.43, 108.45, 72.07, 63.47, 56.51, 52.48, 51.39, 44.20, 43.81, 38.46, 35.85, 17.95, 16.83, 14.86. HRMS calculated for C₂₈H₂₈O₈: [M-H]⁻: 491.1704 (found); 491.1711 (calc). Melting point 104-108 °C.

Methyl-(2*S*,4*aR*,6*aR/S*,7*R*,10*aR*,10*bR*)-2-(furan-3-yl)-9-hydroxy-6*a*,10*b*-dimethyl-4,10-dioxo-2,4,4*a*,5,6,6*a*,7,10,10*a*,10*b*-decahydro-1*H*-benzo[*ff*]isochromene-7-carboxylate (**7a**) Methyl-(2*S*,4*aR*,6*aS*,7*R*,10*bS*)-2-(furan-3-yl)-10-hydroxy-6*a*,10*b*-dimethyl-4,9-dioxo-1,4,4*a*,5,6,6*a*,7,8,9,10*b*-decahydro-2*H*-benzo[*ff*]isochromene-7-carboxylate (**7b**). A combination of CH₂Cl₂ (40 mL) and MeOH (40 mL) was added to a flask containing **6** (250 mg, 0.640 mmol) and Cu(OAc)₂ (349 mg, 1.92 mmol). After stirring overnight at RT the reaction was concentrated in vacuo. The residue was re-dissolved in CH₂Cl₂ (40 mL) and H₂O (40 mL). The aqueous layer was re-extracted with CH₂Cl₂ (2 ×40 mL). The combined organic layers were washed with saturated NH₄Cl (50 mL) and brine (50 mL) then dried over Na₂SO₄. The solvent was removed in vacuo and the residue purified FCC eluting with 12.5% EtOAc/CH₂Cl₂ to yield **7a** and **7b** as a 3:1 mixture (139 mg, 52%) as a white solid. ¹H NMR for **7a** (500 MHz, CDCl₃) δ 7.44 (m, 1H), 7.42 (m, 1H), 6.41 (dd, *J* = 0.80, 1.79 Hz, 1H), 6.02 (d, *J* = 2.50 Hz, 1H),

1 5.59 (dd, $J = 5.25, 11.62$ Hz, 1H), 3.76 (s, 3H), 3.41 (d, $J = 2.49$ Hz, 1H), 3.14 (dd, $J = 5.13, 13.35$ Hz,
2 1H), 2.33 (s, 1H), 2.18 (m, 2H), 2.01 (m, 1H), 1.67 (m, 3H), 1.36 (s, 3H), 1.11 (s, 3H). ^{13}C NMR (126
3 MHz, CDCl_3) δ 194.70, 171.32, 171.25, 146.69, 143.77, 139.38, 125.46, 112.18, 108.42, 71.92, 62.70,
4 55.98, 52.24, 51.27, 44.67, 43.88, 38.20, 35.78, 17.86, 16.64, 14.72. HRMS calculated for $\text{C}_{21}\text{H}_{24}\text{O}_7$:
5 $[\text{M}+\text{Na}]^+$: 411.1409 (found); 411.1420 (calc). Melting point: 165-170 °C (dec).
6
7
8
9
10
11

12 To an ice cold stirring suspension of **6** (140 mg, 0.36 mmol) in methanol (3 mL) and benzene (12 mL),
13 lead tetraacetate (213 mg, 0.48 mmol) was added in four portions over 30 minutes producing a deep red
14 solution that slowly faded to transparent pale yellow as the reaction came to room temperature and stirred
15 overnight. The reaction was quenched by addition of 1M $\text{Na}_2\text{S}_2\text{O}_3$ (15 mL) and sat. NaHCO_3 (15 mL).
16 The resulting mixture stirred for 30 minutes and was then extracted with EtOAc (3 x 25 mL). The
17 combined organic extracts were washed with brine (50 mL), dried (Na_2SO_4) and concentrated. The
18 solvent was removed in vacuo and the residue purified FCC eluting with 12.5% EtOAc/ CH_2Cl_2 to yield
19 **7b** (35 mg, 25 %) as a white crystalline solid. $R_f = 0.6$ (8 % EtOAc / CH_2Cl_2).
20
21
22
23
24
25
26
27
28
29
30

31 ^1H NMR for **7b** (500 MHz, CDCl_3) δ 7.49 - 7.42 (m, 2H), 6.79 (s, 1H), 6.45 (dd, $J = 1.9, 0.9$ Hz, 1H),
32 5.59 (ddd, $J = 10.5, 6.4, 1.1$ Hz, 1H), 3.75 (s, 3H), 3.75 - 3.73 (m, 1H), 3.19 - 3.08 (m, 1H), 3.11 - 3.01
33 (m, 1H), 2.74 (dd, $J = 17.3, 3.0$ Hz, 1H), 2.46 (dd, $J = 12.4, 3.0$ Hz, 1H), 2.22 (dq, $J = 14.2, 3.4$ Hz, 1H),
34 2.16 - 2.03 (m, 1H), 1.80 (tdd, $J = 14.0, 12.3, 3.0$ Hz, 1H), 1.71 (dt, $J = 13.6, 3.2$ Hz, 1H), 1.46 (s, 3H),
35 1.43 (s, 3H), 1.27 (s, 1H). ^{13}C NMR (126 MHz, CDCl_3) δ 192.99, 171.84, 171.70, 143.82, 139.36, 139.25,
36 126.03, 108.62, 71.54, 52.00, 51.74, 50.57, 41.53, 38.64, 37.94, 37.24, 34.82, 29.72, 24.44, 19.02, 17.77.
37 HRMS calculated for $\text{C}_{21}\text{H}_{24}\text{O}_7$: $[\text{M}+\text{H}]^+$: 389.1606 (found); 389.1595 (calc). Melting point: = 215-216
38 °C (dec).
39
40
41
42
43
44
45
46
47
48
49

50 **Synthesis of analogues.** Analogues of **2** were prepared with a MiniBlox XT Parallel Synthesizer to
51 acylate **6** with various benzoyl chlorides using an analogous procedure described for the synthesis of **5**.
52 Analogues of **5** were prepared by EDC and DMAP-mediated couplings of **7** with various benzoic acids.
53
54
55
56
57
58
59
60

1 Full synthetic procedures and full characterization of compounds are provided in the Supplementary
2 Information.
3

4
5 **Calculated properties.** Optimized structures of the compounds were generated in Maestro using the
6 OPLS_2005 force field at pH=7.4. Properties of the optimized structures were calculated using QikProp.¹⁸
7
8

9
10 ***In vitro* pharmacology. Cell lines and cell culture.** The HitHunterTM Chinese hamster ovary cells
11 (CHO-K1) stably expressing the human μ -opioid receptor (OPRM1, catalog # 95-0107C2) the human κ -
12 opioid receptor (OPRK1, catalog # 95-0088C2), or the human δ -opioid receptor, (OPRD1, catalog # 95-
13 0108C2) and the PathHunterTM Chinese hamster ovary cells stably expressing the human μ -opioid
14 receptor β -arrestin-2 EFC cell line (catalog # 93-0213C2) were purchased from DiscoverX Corp.
15 (Fremont, CA) and maintained in F-12 media with 10% fetal bovine serum (Life Technologies, Grand
16 Island, NY), 1% penicillin/streptomycin/ L-glutamine (Life Technologies), and 800 μ g/mL Geneticin
17 (Mirus Bio, Madison, WI). The media of the PathHunterTM cells was supplemented with an additional
18 250 μ g/mL Hygromycin B (Mirus Bio). All cells were grown at 37 °C and 5% CO₂ in a humidified
19 incubator.
20
21
22
23
24
25
26
27
28
29
30
31
32

33
34
35 ***Forskolin-induced cAMP accumulation.*** Assays proceeded as previously described.¹⁵
36
37

38 ***β -arrestin-2 EFC recruitment assay.*** The MOR agonist-mediated β -arrestin-2 recruitment was
39 measured using the DiscoverX PathHunterTM technology. On day 1, ~80% confluent CHO-K1 OPRM1
40 β -arrestin-2 cells were detached from culture plates using nonenzymatic cell dissociation buffer (Life
41 Technologies) and counted using a hemocytometer. Cells were plated at 5 000 cells/well in 20 μ L of Cell
42 Plating Reagent 2 (DiscoverRx) in 384-well tissue culture plates and incubated at 37 °C overnight. On day
43 2, stock solutions of test compounds were generated in 100% DMSO to 5 mM. The stock solutions were
44 used to make 11 serial dilutions and then diluted to yield 5x compound concentrations in assay buffer
45 (Hank's Balanced Salt Solution [HBSS, Life Technologies] with 10 mM HEPES [Life Technologies]).
46 The cells were treated with 5 μ L of the test compound solutions, final concentration of 1X compound and
47 1% DMSO. Cells were incubated for 90 minutes at 37°C. Cells were then treated with detection reagents,
48
49
50
51
52
53
54
55
56
57
58
59
60

12.5 μL per well, according to manufacturer's instructions and incubated at room temperature for at least 1 h protected from light. Luminescence was quantified using a Synergy 2 plate reader with Gen5 Software (BioTek, Winooski, VT). Data were normalized to vehicle (no compound, 1% DMSO final concentration) to remove any background luminescence. The highest dose(s) of DAMGO was used as 100% recruitment and all data was converted to percentages based upon the DAMGO response.

Data analysis. Data were analyzed using nonlinear regression analysis in GraphPad Prism 5.0 software (GraphPad, La Jolla, CA) to generate sigmoidal dose-response curves for both the cAMP accumulation assay and the β -arrestin-2 recruitment assay. cAMP accumulation data were normalized to vehicle and forskolin only control values, and β -arrestin-2 recruitment data were normalized to vehicle and DAMGO maximum response values. All compounds were run in parallel assays in triplicate in ≥ 2 individual experiments. EC_{50} and E_{max} values are reported as the means \pm S.E.M. and represent the average of each individual experiment following nonlinear regression analysis. Bias factors were calculated using relative activity values, as shown in equation 1,

$$\log(\text{Bias Factor}) = \left(\log \left(\frac{E_{\text{max}}_{\text{test}} * \text{EC}_{50}_{\text{DAMGO}}}{\text{EC}_{50}_{\text{test}} * E_{\text{max}}_{\text{DAMGO}}} \right) \right)_{\beta\text{-arrestin}} - \left(\log \left(\frac{E_{\text{max}}_{\text{test}} * \text{EC}_{50}_{\text{DAMGO}}}{\text{EC}_{50}_{\text{test}} * E_{\text{max}}_{\text{DAMGO}}} \right) \right)_{\text{cAMP}} \quad (\text{Eq. 1})$$

Metadynamics simulations. Simulations were performed using protocols that have been reported previously.²¹ Full computational details are presented in the Supporting Information.

Animal studies. Adult male B6-SJL mice (22-29 g) and male Sprague Dawley rats (240-350 g) were housed on a 12 h light cycle and experiments were conducted during the light cycle. All animals were bred and housed at the Victoria University of Wellington (VUW) small animal facility, New Zealand. All experimental procedures were approved by the VUW Animal Ethics Committee and carried out in accordance to their guidelines for animal care. Food and water were provided *ad libitum* except during experimental procedures.

Hot water tail-flick assay. The tail-flick assay was carried out in mice as previously described.²⁸ Briefly, mice were habituated in a plexi-glass restrainer (internal diameter 24 mm) for 15 min for 2 days prior to

1 testing. Latencies were recorded by immersing one third of the tail in a water bath (50 ± 0.5 °C) and
2 measuring the time taken to show a withdrawal response. To avoid tissue damage, the maximum time for
3 the tail immersion was set at 10 s. Control latencies were measured in triplicate before testing and an
4 average calculated.
5
6
7
8

9 To measure the duration of action of anti-nociceptive effects, mice were administered a single dose of
10 compound, morphine sulphate (Hospira New Zealand Limited) or vehicle (dimethyl sulfoxide
11 (DMSO):Tween-80:saline at a ratio of 2:1:7; i.p.) and the withdrawal latencies repeatedly measured at 1,
12 5, 10, 15, 30, 45, 60, 90 and 120 min. The maximum possible effect (MPE) was calculated using the
13 following formula: $\%MPE = 100 \times (\text{test latency} - \text{control latency}) / (10 - \text{control latency})$.
14
15
16
17
18
19
20

21 *Dose-dependent antinociceptive and tolerance evaluation:* The cumulative dose-response tail-flick
22 assay was carried out in mice following repeated daily subcutaneous (s.c.) administration of either
23 Morphine or **5** (10 mg/kg) for 9 days as previously as previously described.²⁷
24
25
26
27

28 *Accelerating rotarod performance assay.* To evaluate motor incoordination, mice were assessed in an
29 accelerating rotarod protocol using previously described protocols,²⁹ Full experimental description are
30 provided in the Supplementary Information.
31
32
33
34

35 *Conditioned place preference assay.* Methods were conducted as previously described,³⁰ and a more
36 detailed description can be found in the Supplementary Information.
37
38
39
40
41
42
43
44
45
46
47
48
49
50
51
52
53
54
55
56
57
58
59
60

Associated Content

Supporting Information. Data includes ^1H NMR, and ^{13}C NMR spectra of **1b**, **4**, **7a-b**, **8a-16a**, and **8b-22b**, ^1H NMR, ^{13}C NMR, COSY, HSQC, and HMBC spectra for **5**, HPLC chromatograms for **1b**, **2**, **4**, **5**, **8a-17a**, and **8b-22b**, further experimental details, and supplementary figures and tables. This material is available free of charge via the Internet at <http://pubs.acs.org>.

Author Information

Corresponding Author. Phone (785) 864-3267. Fax: (785) 864-5326. E-mail: prisinza@ku.edu.

Notes. The University of Kansas has filed a provisional patent related to this work. Other than this, the authors declare no competing financial interests.

Acknowledgements. This work was supported by DA018151 and GM111385 (to TEP), DA03049, MH107053, and DA026434 (to MF), GM008545 (to APR and RSC), AFPE Pre-doctoral Fellowship in Pharmaceutical Sciences (to RSC), and the Neurological Foundation and Health Research Council of New Zealand and Victoria University of Wellington (to BMK). Support for the NMR instrumentation was provided by NIH Shared Instrumentation Grant #S10RR024664 and NSF Major Research Instrumentation Grant #0320648. Computations were run on resources available through the Scientific Computing Facility at Mount Sinai and the Extreme Science and Engineering Discovery Environment (XSEDE) under MCB080109N (to MF), which is supported by National Science Foundation grant number ACI-1053575. The content is the sole responsibility of the authors and does not necessarily represent the official views of the National Institute on Drug Abuse, National Institutes of Health, or the National Science Foundation. The authors would like to thank Dr. Jeff Aubé, Dr. Sudeshna Roy, and Dr. Edward Stahl for their assistance.

References

- 1
2
3
4 1. (a) Institute of Medicine (U.S.). Committee on Advancing Pain Research Care and Education.
5
6 Relieving Pain in America : A Blueprint for Transforming Prevention, Care, Education, and Research.
7
8 National Academies Press: Washington, D.C., 2011; p xvii.; (b) Stein, C. Opioids, sensory systems and
9
10 chronic pain. *Eur. J. Pharmacol.* **2013**, *716*, 179-187.
11
12
- 13
14 2. Center for Behavioral Health Statistics and Quality. *2014 National Survey on Drug Use and Health:*
15
16 *Detailed Tables*. Substance Abuse and Mental Health Services Administration, Rockville, MD. **2015**.
17
18
- 19
20 3. Rudd, R. A.; Aleshire, N.; Zibbell, J. E.; Gladden, R. M. Increases in drug and opioid overdose deaths
21
22 - United States, 2000-2014. *MMWR Morb. Mortal. Wkly. Rep.* **2016**, *64*, 1378-1382.
23
24
- 25
26 4. (a) Williams, D. A.; Roche, V. F.; Roche, E. B. *Foye's Principles of Medicinal Chemistry*. 7th ed.;
27
28 Wolters Kluwer Health/Lippincott Williams & Wilkins: Philadelphia, 2013; p 658-699; (b) Casy, A. F.;
29
30 Parfitt, R. T. *Opioid Analgesics : Chemistry and Receptors*. Plenum Press: New York, 1986.
31
32
- 33
34 5. Blake, H.; Leighton, P.; van der Walt, G.; Ravenscroft, A. Prescribing opioid analgesics for chronic
35
36 non-malignant pain in general practice - a survey of attitudes and practice. *Br. J. Pain* **2015**, *9*, 225-232.
37
38
- 39
40 6. (a) Mansour, A.; Taylor, L. P.; Fine, J. L.; Thompson, R. C.; Hoversten, M. T.; Mosberg, H. I.;
41
42 Watson, S. J.; Akil, H. Key residues defining the mu-opioid receptor binding pocket: a site-directed
43
44 mutagenesis study. *J. Neurochem.* **1997**, *68*, 344-353; (b) Surratt, C. K.; Johnson, P. S.; Moriwaki, A.;
45
46 Seidleck, B. K.; Blaschak, C. J.; Wang, J. B.; Uhl, G. R. -mu opiate receptor. Charged transmembrane
47
48 domain amino acids are critical for agonist recognition and intrinsic activity. *J. Biol. Chem.* **1994**, *269*,
49
50 20548-20553.
51
52
- 53
54 7. Cunningham, C. W.; Rothman, R. B.; Prisinzano, T. E. Neuropharmacology of the naturally
55
56 occurring kappa-opioid hallucinogen salvinorin A. *Pharmacol. Rev.* **2011**, *63*, 316-347.
57
58
59
60

- 1
2
3
4
5
6
7
8
9
10
11
12
13
14
15
16
17
18
19
20
21
22
23
24
25
26
27
28
29
30
31
32
33
34
35
36
37
38
39
40
41
42
43
44
45
46
47
48
49
50
51
52
53
54
55
56
57
58
59
60
8. Beguin, C.; Richards, M. R.; Li, J. G.; Wang, Y.; Xu, W.; Liu-Chen, L. Y.; Carlezon, W. A., Jr.; Cohen, B. M. Synthesis and in vitro evaluation of salvinorin A analogues: effect of configuration at C(2) and substitution at C(18). *Bioorg. Med. Chem. Lett.* **2006**, *16*, 4679-4685.
9. Harding, W. W.; Tidgewell, K.; Byrd, N.; Cobb, H.; Dersch, C. M.; Butelman, E. R.; Rothman, R. B.; Prisinzano, T. E. Neoclerodane diterpenes as a novel scaffold for mu opioid receptor ligands. *J. Med. Chem.* **2005**, *48*, 4765-4771.
10. Groer, C. E.; Tidgewell, K.; Moyer, R. A.; Harding, W. W.; Rothman, R. B.; Prisinzano, T. E.; Bohn, L. M. An opioid agonist that does not induce mu-opioid receptor--arrestin interactions or receptor internalization. *Mol. Pharmacol.* **2007**, *71*, 549-557.
11. (a) Tidgewell, K.; Groer, C. E.; Harding, W. W.; Lozama, A.; Schmidt, M.; Marquam, A.; Hiemstra, J.; Partilla, J. S.; Dersch, C. M.; Rothman, R. B.; Bohn, L. M.; Prisinzano, T. E. Herkinorin analogues with differential beta-arrestin-2 interactions. *J. Med. Chem.* **2008**, *51*, 2421-2431; (b) Xu, H.; Wang, X.; Partilla, J. S.; Bishop-Mathis, K.; Benaderet, T. S.; Dersch, C. M.; Simpson, D. S.; Prisinzano, T. E.; Rothman, R. B. Differential effects of opioid agonists on G protein expression in CHO cells expressing cloned human opioid receptors. *Brain Res. Bull.* **2008**, *77*, 49-54; (c) Rowan, M. P.; Bierbower, S. M.; Eskander, M. A.; Szteyn, K.; Por, E. D.; Gomez, R.; Veldhuis, N.; Bunnett, N. W.; Jeske, N. A. Activation of mu opioid receptors sensitizes transient receptor potential vanilloid type 1 (TRPV1) via beta-arrestin-2-mediated cross-talk. *PLoS One* **2014**, *9*, e93688.
12. (a) Butelman, E. R.; Rus, S.; Simpson, D. S.; Wolf, A.; Prisinzano, T. E.; Kreek, M. J. The effects of herkinorin, the first mu-selective ligand from a salvinorin A-derived scaffold, in a neuroendocrine biomarker assay in nonhuman primates. *J. Pharmacol. Exp. Ther.* **2008**, *327*, 154-160; (b) Lamb, K.; Tidgewell, K.; Simpson, D. S.; Bohn, L. M.; Prisinzano, T. E. Antinociceptive effects of herkinorin, a MOP receptor agonist derived from salvinorin A in the formalin test in rats: new concepts in mu opioid receptor pharmacology: from a symposium on new concepts in mu-opioid pharmacology. *Drug Alcohol*

1
2
3
4
5
6
7
8
9
10
11
12
13
14
15
16
17
18
19
20
21
22
23
24
25
26
27
28
29
30
31
32
33
34
35
36
37
38
39
40
41
42
43
44
45
46
47
48
49
50
51
52
53
54
55
56
57
58
59
60

Depend. **2012**, *121*, 181-188; (c) Ji, F.; Wang, Z.; Ma, N.; Riley, J.; Armstead, W. M.; Liu, R. Herkinorin dilates cerebral vessels via kappa opioid receptor and cyclic adenosine monophosphate (cAMP) in a piglet model. *Brain Res.* **2013**, *1490*, 95-100.

13. Harding, W. W.; Schmidt, M.; Tidgewell, K.; Kannan, P.; Holden, K. G.; Gilmour, B.; Navarro, H.; Rothman, R. B.; Prisinzano, T. E. Synthetic studies of neoclerodane diterpenes from *Salvia divinorum*: semisynthesis of salvinicins A and B and other chemical transformations of salvinorin A. *J. Nat. Prod.* **2006**, *69*, 107-112.

14. (a) Shigehisa, H.; Mizutani, T.; Tosaki, S. Y.; Ohshima, T.; Shibasaki, M. Formal total synthesis of (+)-wortmannin using catalytic asymmetric intramolecular aldol condensation reaction. *Tetrahedron* **2005**, *61*, 5057-5065; (b) Kotoku, N.; Sumii, Y.; Kobayashi, M. Stereoselective synthesis of core structure of cortistatin A. *Org. Lett.* **2011**, *13*, 3514-3517.

15. Riley, A. P.; Groer, C. E.; Young, D.; Ewald, A. W.; Kivell, B. M.; Prisinzano, T. E. Synthesis and kappa-opioid receptor activity of furan-substituted salvinorin A analogues. *J. Med. Chem.* **2014**, *57*, 10464-10475.

16. Groer, C. E.; Schmid, C. L.; Jaeger, A. M.; Bohn, L. M. Agonist-directed interactions with specific beta-arrestins determine mu-opioid receptor trafficking, ubiquitination, and dephosphorylation. *J. Biol. Chem.* **2011**, *286*, 31731-31741.

17. (a) Free, R. B.; Chun, L. S.; Moritz, A. E.; Miller, B. N.; Doyle, T. B.; Conroy, J. L.; Padron, A.; Meade, J. A.; Xiao, J.; Hu, X.; Dulcey, A. E.; Han, Y.; Duan, L.; Titus, S.; Bryant-Genevier, M.; Barnaeva, E.; Ferrer, M.; Javitch, J. A.; Beuming, T.; Shi, L.; Southall, N. T.; Marugan, J. J.; Sibley, D. R. Discovery and characterization of a G protein-biased agonist that inhibits beta-arrestin recruitment to the D2 dopamine receptor. *Mol. Pharmacol.* **2014**, *86*, 96-105; (b) Kenakin, T.; Christopoulos, A. Signalling bias in new drug discovery: detection, quantification and therapeutic impact. *Nat. Rev. Drug Discovery* **2013**, *12*, 205-216; (c) Kenakin, T.; Watson, C.; Muniz-Medina, V.; Christopoulos, A.; Novick, S. A simple

- method for quantifying functional selectivity and agonist bias. *ACS Chem. Neurosci.* **2012**, *3*, 193-203;
- (d) Luttrell, L. M.; Maudsley, S.; Bohn, L. M. Fulfilling the promise of "biased" G protein-coupled receptor agonism. *Mol. Pharmacol.* **2015**, *88*, 579-588; (e) Zhou, L.; Lovell, K. M.; Frankowski, K. J.; Slauson, S. R.; Phillips, A. M.; Streicher, J. M.; Stahl, E.; Schmid, C. L.; Hodder, P.; Madoux, F.; Cameron, M. D.; Prisinzano, T. E.; Aube, J.; Bohn, L. M. Development of functionally selective, small molecule agonists at kappa opioid receptors. *J. Biol. Chem.* **2013**, *288*, 36703-36716.
18. *Small-Molecule Drug Discovery Suite 2015-4: QikProp*, version 4.6; Schrödinger, LLC: New York, NY, 2015.
19. (a) Raiteri, P.; Laio, A.; Gervasio, F. L.; Micheletti, C.; Parrinello, M. Efficient reconstruction of complex free energy landscapes by multiple walkers metadynamics. *J. Phys. Chem. B* **2006**, *110*, 3533-3539; (b) Barducci, A.; Bussi, G.; Parrinello, M. Well-tempered metadynamics: a smoothly converging and tunable free-energy method. *Phys. Rev. Lett.* **2008**, *100*, 020603.
20. Provasi, D.; Bortolato, A.; Filizola, M. Exploring molecular mechanisms of ligand recognition by opioid receptors with metadynamics. *Biochemistry* **2009**, *48*, 10020-10029.
21. Schneider, S.; Provasi, D.; Filizola, M. The dynamic process of drug-GPCR binding at either orthosteric or allosteric sites evaluated by metadynamics. *Methods Mol. Biol.* **2015**, *1335*, 277-294.
22. Neilan, C. L.; Husbands, S. M.; Breeden, S.; Ko, M. C.; Aceto, M. D.; Lewis, J. W.; Woods, J. H.; Traynor, J. R. Characterization of the complex morphinan derivative BU72 as a high efficacy, long-lasting mu-opioid receptor agonist. *Eur. J. Pharmacol.* **2004**, *499*, 107-116.
23. Huang, W.; Manglik, A.; Venkatakrisnan, A. J.; Laeremans, T.; Feinberg, E. N.; Sanborn, A. L.; Kato, H. E.; Livingston, K. E.; Thorsen, T. S.; Kling, R. C.; Granier, S.; Gmeiner, P.; Husbands, S. M.; Traynor, J. R.; Weis, W. I.; Steyaert, J.; Dror, R. O.; Kobilka, B. K. Structural insights into micro-opioid receptor activation. *Nature* **2015**, *524*, 315-321.

- 1
2
3
4
5
6
7
8
9
10
11
12
13
14
15
16
17
18
19
20
21
22
23
24
25
26
27
28
29
30
31
32
33
34
35
36
37
38
39
40
41
42
43
44
45
46
47
48
49
50
51
52
53
54
55
56
57
58
59
60
24. Ballesteros, J. A.; Weinstein, H. Integrated methods for the construction of three-dimensional models and computational probing of structure-function relations in G protein-coupled receptors. *Methods Neurosci.* **1995**, *25*, 366-428.
25. Basbaum, A. I.; Fields, H. L. Endogenous pain control systems: brainstem spinal pathways and endorphin circuitry. *Annu. Rev. Neurosci.* **1984**, *7*, 309-338.
26. Trang, T.; Al-Hasani, R.; Salvemini, D.; Salter, M. W.; Gutstein, H.; Cahill, C. M. Pain and poppies: the good, the bad, and the ugly of opioid analgesics. *J. Neurosci.* **2015**, *35*, 13879-13888.
27. Bohn, L. M.; Gainetdinov, R. R.; Lin, F. T.; Lefkowitz, R. J.; Caron, M. G. Mu-opioid receptor desensitization by beta-arrestin-2 determines morphine tolerance but not dependence. *Nature* **2000**, *408*, 720-723.
28. Simonson, B.; Morani, A. S.; Ewald, A. W. M.; Walker, L.; Kumar, N.; Simpson, D.; Miller, J. H.; Prisinzano, T. E.; Kivell, B. M. Pharmacology and anti-addiction effects of the novel κ opioid receptor agonist Mesyl Sal B, a potent and long-acting analogue of salvinorin A. *Br. J. Pharmacol.* **2014**, *172*, 515-531.
29. Deacon, R. M. Measuring motor coordination in mice. *J. Visualized Exp.* **2013**, e2609.
30. Piepponen, T. P.; Kivastik, T.; Katajamaki, J.; Zharkovsky, A.; Ahtee, L. Involvement of opioid mu 1 receptors in morphine-induced conditioned place preference in rats. *Pharmacol. Biochem. Behav.* **1997**, *58*, 275-279.

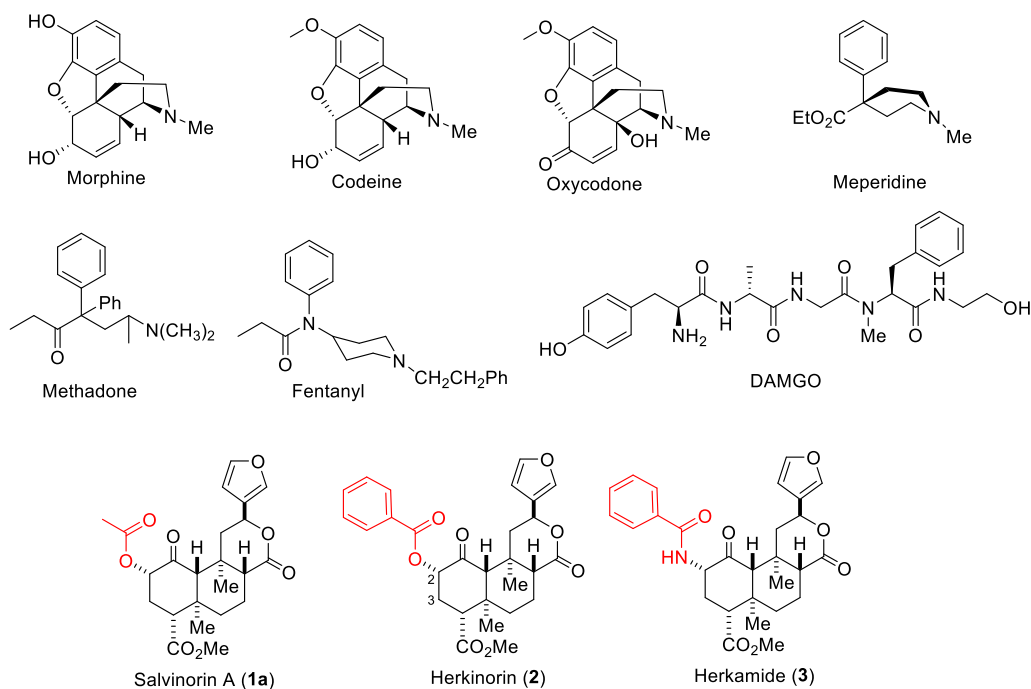
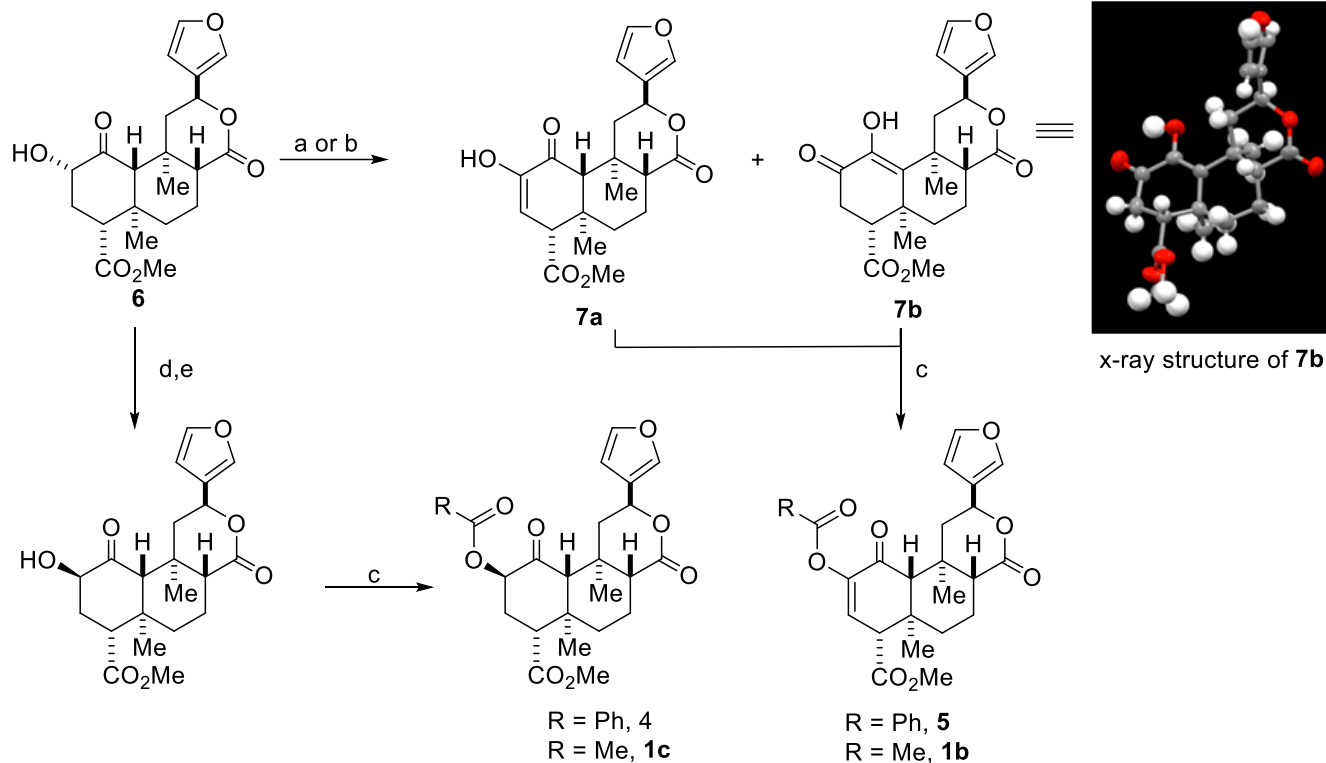


Figure 1. Many opioids are derived structurally from morphine, including codeine, oxycodone, meperidine, methadone, and fentanyl. The structure of traditional MOR agonists morphine and DAMGO differ significantly from those of the KOR agonist salvinorin A (1) and the MOR agonists herkinorin (2) and herkamide (3).

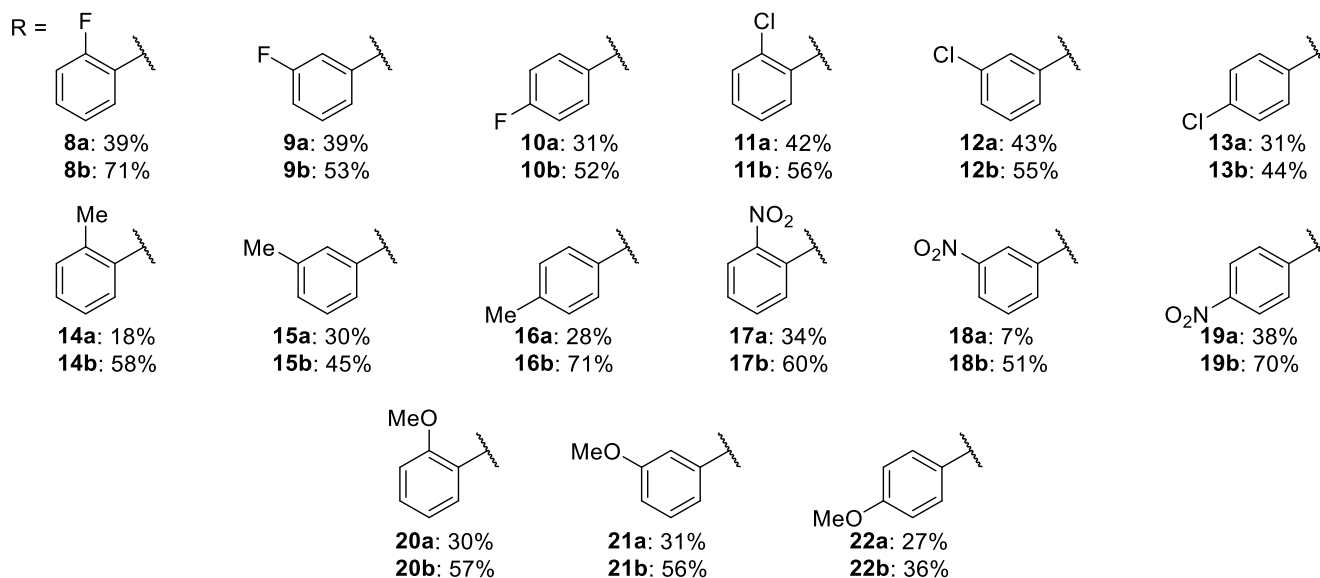
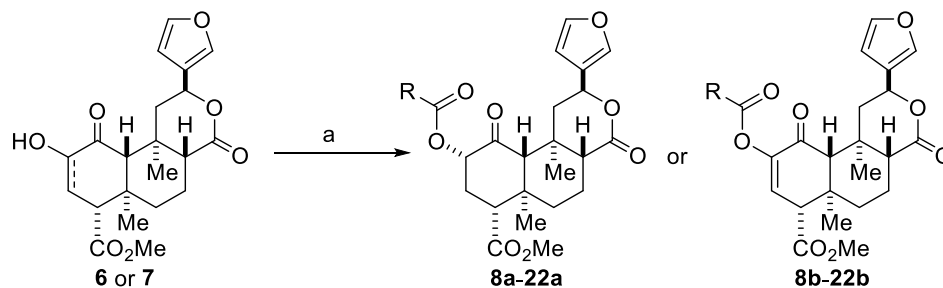


Scheme 1. Synthetic route to compounds **4**, **5**, **1b**, and **1c**. Reagents and conditions: a) $\text{Cu}(\text{OAc})_2$, $\text{MeOH}/\text{CH}_2\text{Cl}_2$ (1:1); b) $\text{Pb}(\text{OAc})_4$, $\text{MeOH}/\text{benzene}$; c) RCOOH or RCOCl , DMAP, DIPEA, CH_2Cl_2 ; d) $p\text{-NO}_2\text{PhCO}_2\text{H}$, DIAD, PPh_3 , CH_2Cl_2 ; e) K_2CO_3 , MeOH .

Table 1. MOR, KOR, and DOR Pharmacology: Inhibition of forskolin-induced cAMP accumulation.

Compound	EC ₅₀ ± SD ^{a, b} (nM)			Selectivity		Calculated values ^g	
	μ	κ	δ	κ/μ	δ/μ	cLogP	PSA (Å ²)
DAMGO	0.60 ± 0.4	>10 000 ^d	ND ^f	>16 000	--	-0.65	198
Morphine	5.0 ± 3	330 ± 200	780 ± 150 ^h	66	150	0.89	58
2	40 ± 10	170 ± 70 ^e	>10 000 ^d	4.25	250	3.46	124
3	3.0 ± 0.6	>10 000 ^d	690 ± 50 ^d	>3 000	210	3.73	131
4	>10 000 ^d	>10 000 ^d	ND ^f	--	--	3.41	129
5	1.2 ± 0.6	>10 000 ^d	74 ± 10	>8 000	63	3.11	130
1a	>10 000 ^d	0.04 ± 0.04	>10 000 ^d	< 4.0E-6	--	2.00	131
1b	>10 000 ^d	0.56 ± 0.2	ND ^f	< 5.6E-5	--	2.24	127
1c	>10 000 ^d	110 ± 30	ND ^f	< 1.1E-2	--	1.62	133
7a^c	>10 000 ^d	4.9 ± 0.5	ND ^f	< 4.9E-4	--	1.90	119
7b	>10 000 ^d	>10 000 ^d	ND ^f	--	--	1.84	121

^aMean ± standard deviation; n ≥ 2 individual experiments run in triplicate. ^bE_{max} = 100% unless otherwise noted. ^cCompound **7a** was tested as a 3:1 mixture with **7b**. ^dE_{max} = 0 % up to 10 μM. ^eE_{max} = 64 ± 18 %. ^fND = Not Determined. ^gValues calculated using QikProp.¹⁸ ^hE_{max} = 90 ± 2%.



31
32
33
34
35
36
37
38
39
40
41
42
43
44
45
46
47
48
49
50
51
52
53
54
55
56
57
58
59
60

Scheme 2. Synthesis of two parallel series of **2** and **5** derivatives. Reagents and conditions: a) RCO₂H (2.0 equiv), EDC·HCl (2.0 equiv), DMAP (2.0 equiv), CH₂Cl₂, RT, 16 h.

Table 2. MOR, KOR, and DOR pharmacology: Inhibition of forskolin-induced cAMP accumulation.

Compound	EC ₅₀ ± SD ^{a, b} (nM)			Selectivity	
	μ	κ	δ	κ/μ	δ/μ
5	1.2 ± 0.6	>10 000 ^d	74 ± 10	>8 000	63
8b	4.8 ± 2	160 ± 50	180 ± 30	33	37
9b	4.7 ± 0.5	>10 000 ^c	140 ± 20	>2 000	30
10b	15 ± 3	260 ± 120	350 ± 60	17	23
13b	30 ± 20	>10 000 ^c	310 ± 15	>330	10
16b	22 ± 1	>10 000 ^c	380 ± 40	>450	17
19b	31 ± 3	>10 000 ^c	770 ± 40	>320	25
21b	11 ± 4	>10 000 ^c	620 ± 100	>900	56
22b	8.0 ± 7	>10 000 ^c	120 ± 20	>1 200	15

^a Mean ± standard deviation; n ≥ 2 individual experiments run in triplicate. ^b E_{max} = 100%, unless noted otherwise. ^c E_{max} = 0 % up to 10 μM.

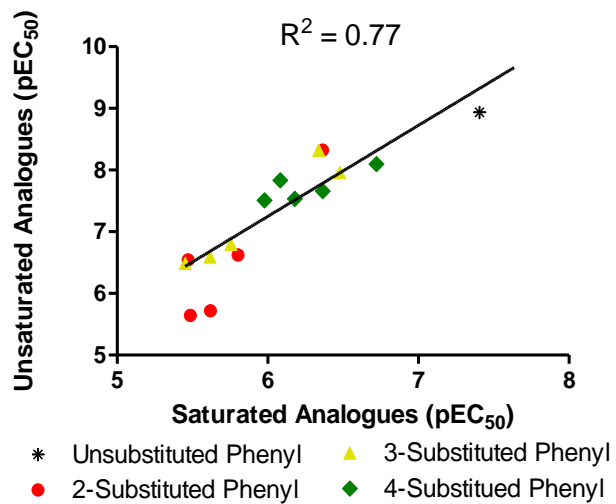


Figure 2. Scatter plot comparison of the pEC₅₀ values of 2 analogues vs. 5 analogues.

Table 3. MOR Pharmacology: MOR-mediated β -arrestin recruitment.

Compound	EC ₅₀ \pm SEM ^a (nM)	% Efficacy \pm SEM ^b	Bias Factor ^c
DAMGO	42 \pm 5	97 \pm 0.9	1.0
Morphine	380 \pm 40	38 \pm 1	0.36
2	3400 \pm 700	72 \pm 3	0.95
3	560 \pm 60	85 \pm 3	0.32
5	140 \pm 40	96 \pm 3	0.57
8b	63 \pm 4	91 \pm 4	5.0
9b	41 \pm 10	79 \pm 2	6.6
10b	200 \pm 70	95 \pm 4	5.2
13b	180 \pm 40	76 \pm 2	9.4
16b	360 \pm 130	110 \pm 6	4.9
19b	330 \pm 70	46 \pm 4	3.2
21b	190 \pm 20	74 \pm 3	3.1
22b	96 \pm 30	76 \pm 3	4.6

^aMean \pm standard error of the mean; n \geq 3 individual experiments run in triplicate. ^bMaximum efficacy values calculated based on DAMGO maximum stimulation. ^cBias factors were calculated using Eq. 1 as described in the Experimental Section. Values <1 indicate bias towards the cAMP pathway and values >1 indicate bias towards the β -arrestin-2 pathway. DAMGO is the reference compound, with a bias = 1.

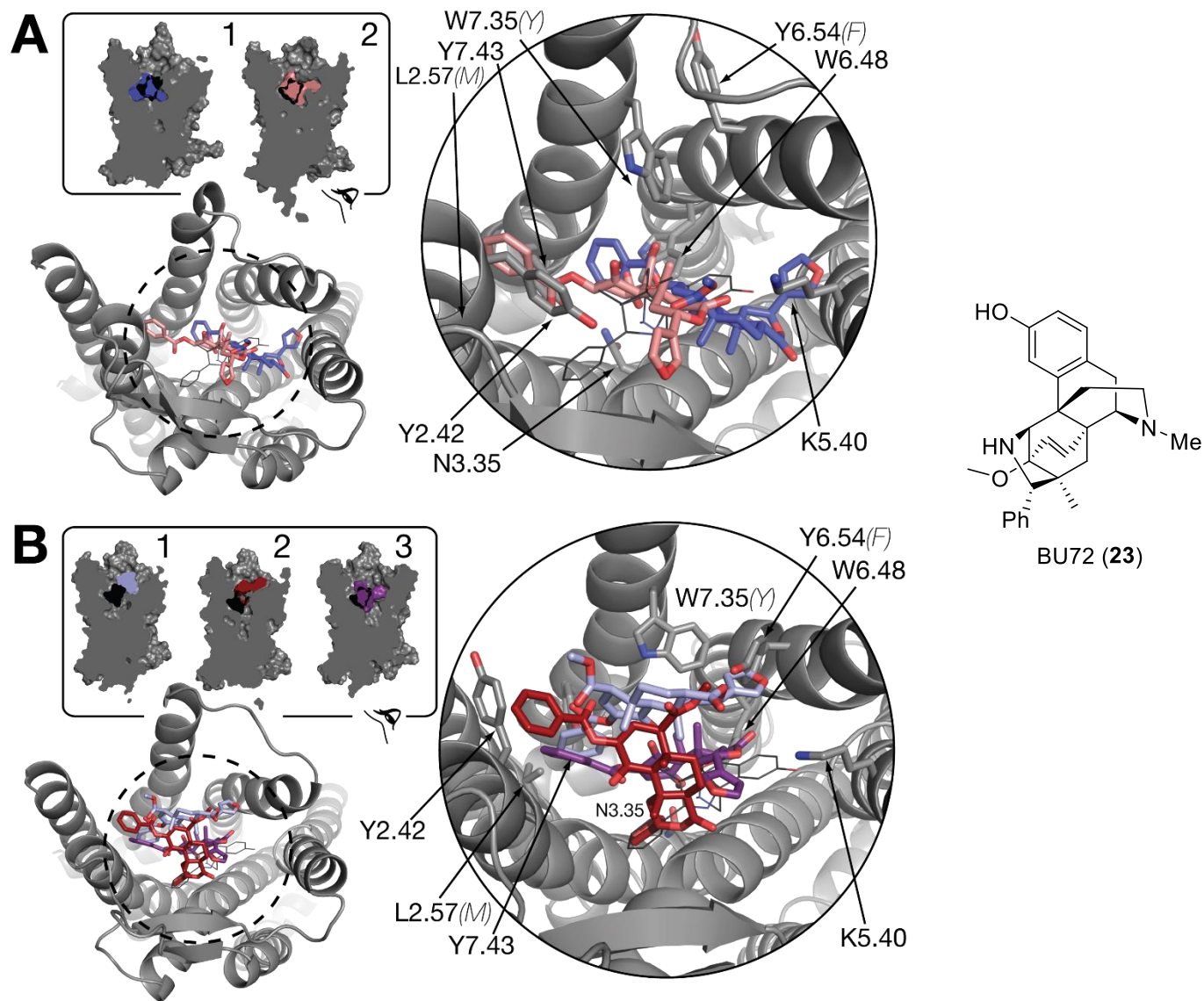


Figure 3. The co-crystallized ligand in the active structure of the μ -opioid receptor **23** is shown in thin black lines. Insets show sections of the receptor and ligand densities in the plane normal to the membrane, and a close up of the ligand-receptor interactions, with key residues shown as gray sticks. Non-conserved residues in the κ -opioid receptor are reported in parentheses. (a) Poses of **2** in clusters 1 and 2 (in blue and pink, respectively). (b) Poses of **5** in clusters 1, 2 and 3 (in light-blue, red, and purple, respectively).

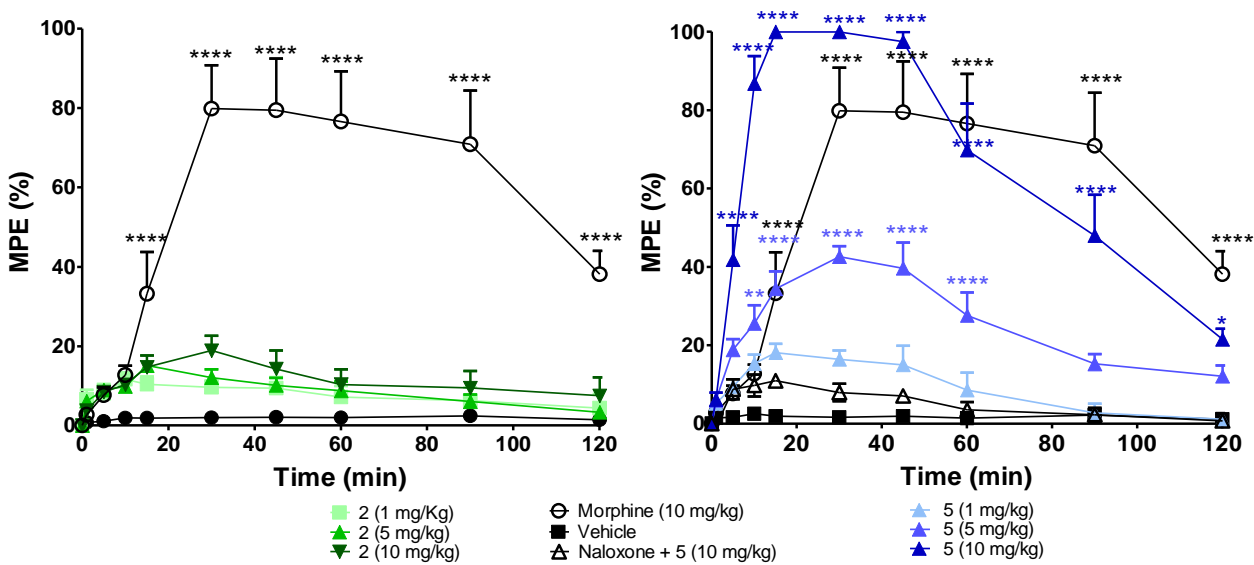


Figure 4. The centrally mediated antinociceptive effects of **2** and **5** were assessed in the hot-water tail-flick assay in mice at 1, 5, and 10 mg/kg, i.p., doses alongside morphine (10 mg/kg) with a 10 s time cutoff to prevent tissue injury. (a) **2** demonstrates no significant antinociceptive effects. (b) At 5 and 10 mg/kg doses, **5** produces significant antinociceptive effects, similar to that of morphine at the 10 mg/kg dose. Data shown as mean \pm SEM ($n=5-10$ per group). **** $p<0.0001$, *** $p<0.001$, ** $p<0.01$, * $p<0.05$, drug compared to vehicle.

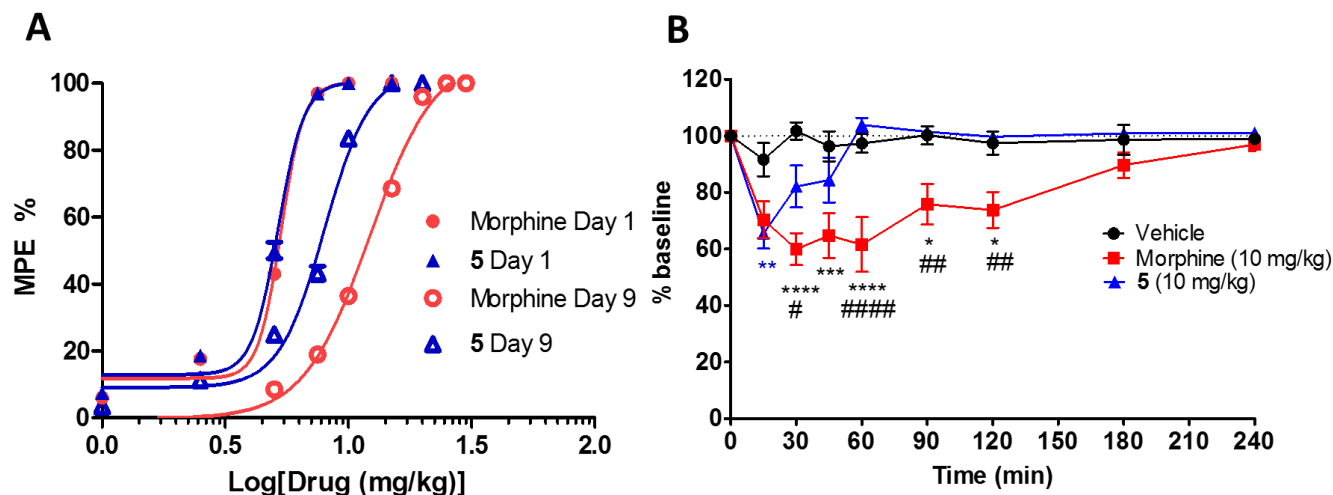


Figure 5. (a) Antinociceptive effects in the hot water tail-flick assay in mice following cumulative dosing on day 1 (filled symbols) and again on day 9 (open symbols) following daily administration of 10 mg/kg/s.c. morphine or 5 ($n=7$). (b) Using a rotarod set to accelerate from 4 to 40 rpm over 300 s, morphine (10 mg/kg/i.p.) showed a significant decrease in motor coordination compared to 5 (10 mg/kg/i.p.) and vehicle ($n=6$) **** $p<0.0001$, *** $p<0.001$, ** $p<0.01$, * $p<0.05$, drug compared to vehicle (b); ##### $p<0.0001$, ### $p<0.001$, ## $p<0.01$, # $p<0.05$, morphine compared to 5. Data shown as mean \pm SEM.

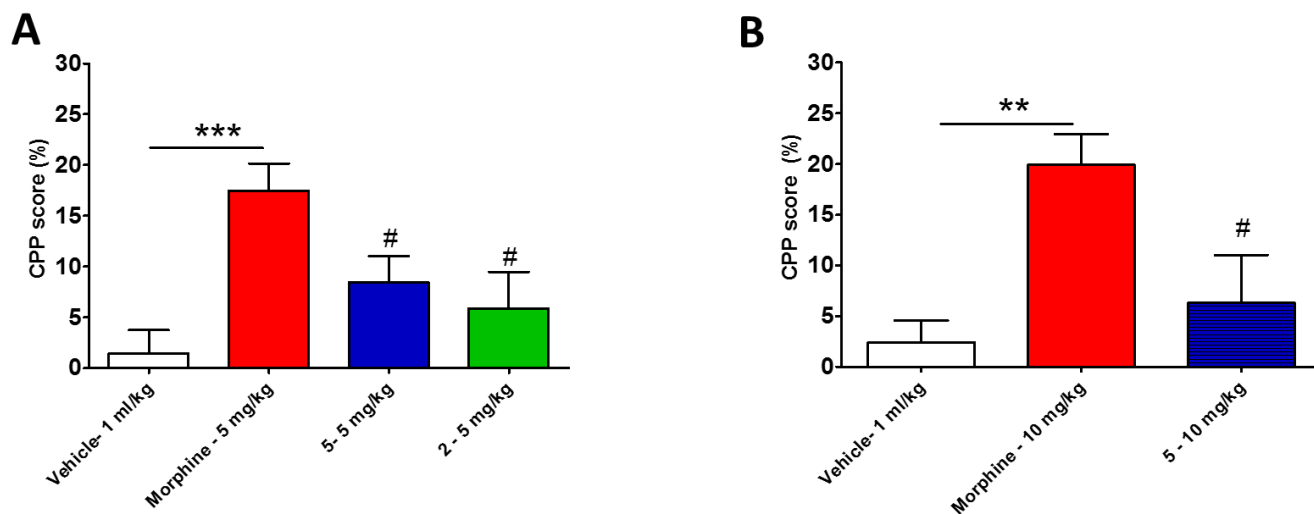


Figure 6. A significant place preference is seen in the morphine paired chamber at both (a) 5 mg/kg, (i.p.), and (b) 10 mg/kg, (i.p.) doses, but not with the same dose of 5 when compared to vehicle. Neither 5 (5 and 10 mg/kg) nor 2 (5 mg/kg) were significantly different to vehicle. (n=8-18). ***p<0.001, **p<0.01 compared to vehicle; #p<0.05 compared to morphine.

Table of Contents Graphic

